Journal of Intelligent & Robotic Systems (2019) 93:151–162
https://doi.org/10.1007/s10846-018-0876-7

Real-Time UAS Guidance for Continuous Curved GNSS Approaches

Alessandro Gardi[1] · **Roberto Sabatini**[1] · **Subramanian Ramasamy**[1] · **Trevor Kistan**[2]

Received: 8 October 2017 / Accepted: 18 May 2018 / Published online: 11 June 2018

Abstract
This paper presents new efficient guidance algorithms allowing Unmanned Aircraft Systems (UAS) to avoid a variety of Global Navigation Satellite System (GNSS) continuity and integrity performance threats detected by an Aircraft Based Augmentation System (ABAS). In particular, the UAS guidance problem is formulated as an optimal control-based Multi-Objective Trajectory Optimization (MOTO) problem subject to suitable dynamic and geometric constraints. Direct transcription methods of the global orthogonal collocation (pseudospectral) family are exploited for the solution of the MOTO problem, generating optimal trajectories for curved GNSS approaches in real-time. Three degrees-of-freedom aircraft dynamics models and suitable GNSS satellite visibility models based on Global Positioning System (GPS) constellation ephemeris data are utilised in the MOTO solution algorithm. The performance of the proposed MOTO algorithm is evaluated in representative simulation case studies adopting the JAVELIN UAS as the reference platform. The paper focusses on descent and initial curved GNSS approach phases in a Terminal Maneuvering Area (TMA) scenario, where multiple manned/unmanned aircraft converge on the same short and curved final GNSS approach leg. The results show that the adoption of MOTO based on pseudospectral methods allows an efficient exploitation of ABAS model-predictive augmentation features in online GNSS guidance tasks, supporting the calculation of suitable arrival trajectories in 7 to 16 s using a normal PC.

Keywords GNSS integrity · GNSS augmentation · Avionics based integrity augmentation · Unmanned aircraft systems · Trajectory optimization · Flight planning

1 Introduction

Realistic Unmanned Aircraft Systems (UAS) flight maneuvers are prone to Global Navigation Satellite Systems (GNSS) outages or severe performance degradations due to the separate or combined effect of various adverse conditions including antenna obscuration, bad satellite geometries, low Carrier-to-Noise ratios (C/N_0), Doppler shifts, interference and multipath [22]. While some of these problems can be mitigated thanks to opportune design provisions (i.e., signal filtering, antenna position optimization, etc.), little can be done to prevent critical signal losses during realistic maneuvers even when considering the availability of Satellite- and Ground-Based Augmentation Systems (SBAS/GBAS). Typically, airworthiness regulations impose stringent GNSS navigation performance requirements, which cannot be fulfilled by current SBAS and GBAS technologies in some of the most demanding operational tasks such as precision approaches or UAS Sense-and-Avoid (SAA) [16, 20, 22]. For instance, the approach and landing phases of both manned aircraft and UAS present a number of challenges as degradations in navigation performance can easily lead to safety-critical conditions. Similar issues can occur in congested airspace sectors where high levels of Required Navigation Performance (RNP) are implemented such as in the case of dense Terminal Maneuvering Areas (TMA), as any departure from the relatively small protection buffers may lead to potential collisions with other traffic. These issues are adequately resolved for manned aircraft either by relying on the manual intervention by the pilot or by integrating high-reliability equipment and implementing adequate levels of redundancy. The first strategy is adopted, for instance, in the case of non-precision

✉ Roberto Sabatini
roberto.sabatini@rmit.edu.au

[1] School of Engineering, RMIT University, Melbourne, VIC 3000, Australia

[2] THALES Australia – Air Traffic Management, Melbourne, VIC 3000, Australia

approaches and up to Category 2 (CAT II) Instrument Landing Systems (ILS), hence with a decision height and a runway visual range of at least 200 ft and 300 m respectively. The second strategy is adopted in the case of Category 3 (CAT III) precision ILS approaches, hence with zero visibility and decision height. However, these strategies are largely unfeasible for UAS. The research community is therefore investigating new technologies and operational measures to enhance the levels of safety of manned aircraft and, most importantly, support the safe operation of UAS in all classes of airspace and in a variety of adverse weather conditions such as in the case of low visibility, cloudiness and precipitations. A very promising strategy to prevent incurring in safety-critical conditions consists in implementing navigation Continuity and Integrity Monitoring and Augmentation (CIMA) technologies on board manned and unmanned aircraft. While considerable work is being done on Receiver-Autonomous Integrity Monitoring (RAIM) technology, this approach has some known limitations [22]. Aircraft-Based Augmentation Systems (ABAS), on the other hand, can support the real-time avoidance of safety-critical flight conditions and a fast recovery of the required navigation performance in case of GNSS data losses. For these reasons, ABAS is well-suited to increase the levels of navigation continuity, integrity and accuracy, complementing RAIM as well as GBAS/SBAS, also known as Local-Area and Wide-Area Augmentation Systems (LAAS/WAAS) to fulfill the stringent requirements for some of the most demanding operational tasks, such as sense-and-avoid, low-visibility landing, etc. [22]. The research community has also recognized a variety of disadvantages associated with the current long, straight and shallow paths followed by instrument flights for precision approach and landing [10, 13]. This shallow approach profile is in fact responsible for operational, environmental and economic inefficiencies and prevent precision approaches to be implemented in topographically-constrained airports [2]. In this respect, the major aviation modernization initiatives around the world (including SESAR/NextGen) are now targeting the required technological and regulatory evolutions that will also support the introduction of steeper and curved precision GNSS approach and landing procedures [15, 23]. The greatest prospective benefits of steeper and curved GNSS approach and landing procedures are related to aircraft noise mitigation strategies in densely inhabited regions and to relieving wake turbulence separation constraints by lateral and vertical displacements of the approach path with respect to the preceding aircraft. Steeper and curved approach procedures crucially rely on satellite navigation technology and on opportune implementations of GBAS, ABAS and 4DT optimization techniques, which are the focus of this article.

This article is an extended version of Gardi and Sabatini [11], addressing some of the key developments required along the research on ABAS to introduce curved and steeper GNSS approaches for both manned aircraft and UAS. In particular, we present a detailed UAS guidance solution considering realistic operational constraints, multiple objectives and targeting the avoidance of GNSS signal degradations. The reference platform for this study is the Javelin (Fig. 1), a small-size fixed-wing UAS belonging to RMIT's unmanned aircraft fleet. The presented solution fulfills not only the conventional constraints for the smoothness of the aircraft trajectory, but also the ones associated with GNSS signal performance. While elements of novelty are also introduced in the set of equations used to model three degrees of freedom aircraft dynamics (particularly by integrating the geometric curvature of the trajectory), the main scientific contributions brought about in our approach are related to the tight integration of GNSS signal degradation models as path constraints in the pseudospectral-based optimal control framework. The results presented in this article demonstrate that our proposed approach is not only technically feasible but can also, if properly implemented, achieve very satisfactory computational performances, indeed very close to the standard 4D trajectory optimization model set used in our research for terminal maneuvering area operations.

2 GBAS and ABAS Overview

GBAS provides differential GNSS corrections and integrity monitoring features at airports where this system is available [22]. GBAS technology is essential to advance GNSS performance in approach beyond ILS CAT I, hence supporting precision approach in low visibility conditions, potentially replacing ILS altogether. This is particularly interesting for UAS manufacturers and operators due to the impracticality of miniaturized high-performance ILS receivers certified for precision approaches onboard unmanned platforms. The availability of GBAS at the considered airport is assumed for precision GNSS approaches, though the guidance techniques presented in this paper can equally

Fig. 1 Javelin UAS

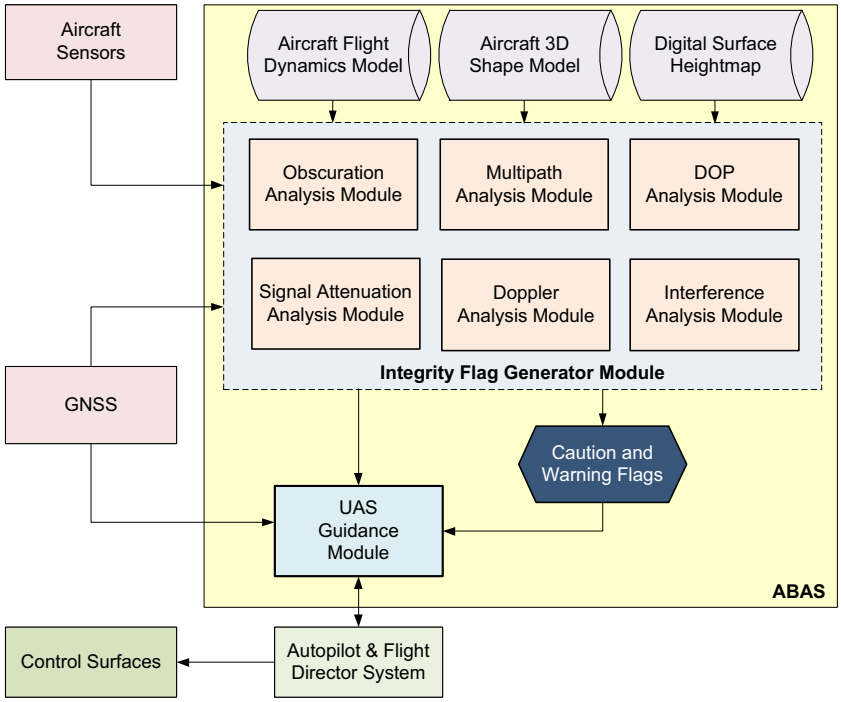

Fig. 2 Top-level ABAS architecture

apply to non-precision GNSS approaches, provided that SBAS is available to support Localizer Performance with Vertical guidance (LPV) approaches or a Vertical Navigation (VNAV)-capable altimeter is equipped on the UAS for Approach with Vertical Guidance (APV) following the so-called baro-VNAV provisions [8]. In both cases, the UAS is assumed to be equipped with an ABAS capable of predicting and/or detecting GNSS signal performance degradations and subsequently initiating a real-time avoidance of safety-critical flight conditions and fast recovery of the required navigation performance. This is performed by implementing two complementary strategies in mission- and safety-critical UAS applications: prediction and avoidance, or reaction and correction. The principles of the ABAS are extensively covered in Sabatini et al. [22]. The architecture of the ABAS for UAS is depicted in Fig. 2. The ABAS does neither require GBAS nor SBAS to be available, though can work synergically with these if available [21].

In case of any predicted or detected GNSS performance threshold violation, ABAS dispatches suitable warning or caution signals to the Autopilot & Flight Director System (A&FDS) and to the human flight crew on board or on the ground, thereby allowing timely correction maneuvers to be performed. Research in ABAS addressed various potential GNSS signal degradations such as the ones associated with antenna obscuration, Doppler shift, multipath, signal-to-noise ratio, jamming and others. Research also evaluated the opportunities of expanding the concept to communication and surveillance systems. In this particular research activity, we focus on Caution/Warning Flags (CF/WF) generated in relation to satellite visibility, masking, Dilution of Precision (DOP) and tracking errors, according to the criteria listed respectively in Tables 1 and 2, where EHE is the Estimated Horizontal Error; EVE is the Estimated Vertical Error; HAL is the Horizontal Alert Limit; VAL is the Vertical Alert Limit; DLL is the Delay Lock Loop; FLL is the Frequency Lock Loop; PLL is the Phase Lock Loop; and T is the pre-detection integration time. These are very important causes of GNSS signal degradation in low altitude maneuvering flight in the TMA. In the implementation presented here, a geometric path constraint on the elevation of satellites in view is introduced in the trajectory optimization model set, as this requirement can simultaneously contribute to prevent errors and losses associated with satellite visibility, masking

Table 1 CF criteria [21]

CF type	CF generation criteria
Satellite visibility	When one satellite elevation angle (in the antenna frame) is less than 10 degrees
Masking	When the current aircraft maneuver will lead to less than 4 satellites in view
DOP	When the $EHE_{3\sigma}$ exceeds the HAL or $EVE_{3\sigma}$ exceeds the VAL
Tracking loops	When either: $42.25^\circ \leq 3\sigma_{PLL} \leq 45^\circ$ or $0.2375T \leq 3\sigma_{FLL} \leq 0.25T$ or $0.05d \leq 3\sigma_{DLL} \leq$ d

Table 2 WF criteria [21]

WF Type	WF generation criteria
Satellite visibility	When one satellite elevation angle (in the antenna frame) is less than 5 degrees
Masking	When less than 4 satellites are in view
DOP	When the $EHE_{2\sigma}$ exceeds the HAL or the $EVE_{2\sigma}$ exceeds the VAL
Tracking loops	When either: $3\sigma_{PLL} > 45°$ or $3\sigma_{FLL} > 1/4T$ or $3\sigma_{DLL} > d$

and DOP and, in conjunction with smooth variations of relative satellite bearing, can also mitigate errors and losses associated with the tracking loops. In particular, the introduced constraint limits the relative deviations of the elevation angle in the receiver antenna reference frame with respect to the initial value (i.e., at the beginning of the approach phase). In our particular case, these deviations from the initial value are constrained not to exceed the interval $[-5°; +10°]$.

3 UAS Guidance Module

The purpose of the UAS guidance algorithm is to find the inputs to the given system characterized by a set of equations of motion and path constraints, which will maximize or minimize specific parameters (e.g., time, fuel consumption, distance from another UAS, relative velocities). As reviewed in great detail in Mujumdar and Padhi [18], Tsourdos et al. [24] a wide variety of tree-based, geometric, kinematic and energy-based methods have been proposed for UAS path-planning, showing notable advantages in various contexts, but these methods are inherently incapable of incorporating complex constraints, such as the ones associated with the attitude of the aircraft. On the other hand, while slightly more complex mathematically and computationally, the Optimal Control Problem (OCP) formulation can natively entail dynamics, geometric and operational constraints. Suitable models, constraints, objectives and numerical OCP solution algorithms can therefore allow determining optimal GNSS lossless flight trajectories. A single-objective OCP is stated as: *determine the states* $\boldsymbol{x}(t)$ *and the controls* $\boldsymbol{u}(t)$ *that optimize the performance index*

$$J = \Phi[\boldsymbol{x}(t_f), \boldsymbol{u}(t_f)] + \int_{t_0}^{t_f} \Psi[\boldsymbol{x}(t), \boldsymbol{u}(t)]dt \tag{1}$$

subject to the dynamic constraints

$$\dot{\boldsymbol{x}}(t) = \boldsymbol{f}[\boldsymbol{x}(t), \boldsymbol{u}(t), t] \tag{2}$$

and to the path constraints

$$\boldsymbol{C}_{\min} \leq \boldsymbol{C}[\boldsymbol{x}(t), \boldsymbol{u}(t), t] \leq \boldsymbol{C}_{\max} \tag{3}$$

where t_0 and t_f are the initial and final time, Φ is the Mayer cost function and Ψ is the Lagrange cost function; f and C represent generic functions, which are at least continuous in t. Initial and boundary conditions are also introduced including minimum, maximum, initial and final values for the various state and control variables involved. In safety-critical applications such as curved and steeper precision GNSS approaches, all the necessary constraints associated to GNSS signal degradations are included in the path constraints and the trajectory is optimized for minimum time and/or fuel to destination waypoint. However, more complex criteria can be set based on the actual aircraft performance parameters (e.g., minimum noise or pollutant emissions) or on the characteristics of the mission (i.e., to maximize distance from conflicting traffic, to minimize the distance from the initial waypoint, etc.). One of the key challenges in the development of online trajectory optimization algorithms is to produce results in real-time (real-time here is intended for the specific application/scenario involved), since the numerical solvers have to be capable of producing accurate and usable outputs in a relatively short time. Optimal control problems can be solved using various methods and the two main categories are direct methods and indirect methods. Direct methods are recently prevailing due to very efficient and accurate discretization schemes. In this class of methods, the UAS dynamics (continuous) variables are translated into a number of discretized state and command parameters. The original OCP is thereby transformed into a finite-dimensional Non-Linear Programming (NLP) problem and the states are implicitly integrated with a quadrature method (or sometimes explicitly integrated) for an arbitrary but finite number of intervals. The most computationally efficient direct collocation methods adopt linearly independent (orthogonal) polynomial functions and are therefore called pseudospectral, and are presented in more detail in Section 3.2.

Planning or optimizing a new trajectory for an UAS is subject to numerous objectives and constraints. Those can be derived from Air Traffic Management (ATM) sequencing and spacing/de-confliction constraints, flight plan/mission objectives, autonomous Separation Assurance and Collision Avoidance (SA/CA), and environmental restrictions/objectives. Thus, the optimization process needs to find the best trade-off between all objectives subject to the dynamics/operational constraints associated with the platform, the planned mission and the current

flight profile/phase. Clearly, different sets of data (from widely differing sources) and significantly different objectives/constraints can be used at the mission planning stage and in real-time flight trajectory optimization tasks. ABAS offer the advantage of meeting the requirements of strategic and tactical air operation tasks, with also the possibility to enhance the performance of SA/CA systems that rely on GNSS as the primary source of navigation data. These include modern cooperative SA/CA systems (e.g., ADS-B) or non-cooperative sensors integrated with GNSS-driven Guidance, Navigation and Control (GNC) systems.

3.1 UAS Flight Dynamics

For the real-time trajectory planning performed by the UAS guidance module we focus on Three Degrees-of-Freedom (3-DoF) dynamics models, which are widely available in the literature and can be derived from Six Degrees-of-Freedom (6-DoF) models as necessary. The 3-DoF model is formulated following a simplified approach based on Newton's second law expressed along the coordinate axes of the body frame and on the motion of such frame with respect to an inertial reference frame of convenience. To simplify the numerical implementation and particularly the operational 4DT realization stage, an alternative formulation of 3-DoF dynamics adopting the geometric trajectory curvature (κ) in place of the bank angle (μ) as the lateral control variable is proposed here. The principal advantage is that the geometric trajectory curvature is the inverse of the local turn radius, which thus can be directly computed from the optimization results. Additionally, while the turn radius feature a mathematical singularity in the admissible domain (i.e., $R \rightarrow \infty$ for straight segments), the curvature does not feature mathematical singularities. The full set of Differential Algebraic Equations (DAE) expressing 3-DoF flight dynamics can be written as:

$$\dot{v} = \frac{T - D}{m} - g \sin\gamma \tag{4}$$

$$\dot{\gamma} = \frac{\mathrm{g}}{v}\left[\left(N^2 - \frac{\kappa^2 v^4 \cos^2\gamma}{g^2}\right)^{\frac{1}{2}} - \cos\gamma\right] \tag{5}$$

$$\dot{\chi} = \kappa \cdot v \tag{6}$$

$$\dot{\phi} = \frac{v\cos\gamma\cos\chi + v_{\mathrm{w}_\phi}}{R_E + Z} \tag{7}$$

$$\dot{\lambda} = \frac{\mathrm{v}\cos\gamma\sin\chi + \mathrm{v}_{\mathrm{w}_\lambda}}{(R_E + z)\cos\phi} \tag{8}$$

$$z = v\sin\gamma + v_{\mathrm{w}_z} \tag{9}$$

$$\dot{m} = -\mathrm{FF} \tag{10}$$

where the state vector consists of: True Air Speed (TAS) v [m s^{-1}], flight path angle γ [deg]; track angle (clockwise from North) χ [deg]; geodetic latitude ϕ [deg]; geodetic longitude λ [deg]; altitude z [m]; aircraft mass m [kg]; whereas the control vector includes: thrust force T [N]; load factor N [ ]; geometric trajectory curvature κ [m^{-1}]. Other variables and parameters include aerodynamic drag D [N]; wind velocity v_w in its three scalar components [m s^{-1}]; gravitational acceleration g [m s^{-2}]; local Earth radius R_E [m]; fuel flow FF [kg s^{-1}]. The aerodynamic drag is modeled as

$$D = \frac{1}{2}\rho v^2 S(C_{D0} + C_{D2}C_L^2) \tag{11}$$

where $\rho = \rho(\phi, \lambda, z, t)$ is the local air density retrieved from weather input data grid or a weather model, S is the reference wing surface, C_{D0} and C_{D2} are the parabolic drag coefficients. The lift coefficient C_L can be calculated from:

$$N\ m\ g = \frac{1}{2}\rho v^2 S C_L \tag{12}$$

The thrust force magnitude is expressed as the product of a throttle coefficient τ (defined as dimensionless and ranging between 0 and 1) and a maximum thrust T_{MAX}, plus an eventual residual thrust term at zero throttle (T_0), as in:

$$T(t) = \tau(t) \cdot T_{MAX} + T_0 \tag{13}$$

In the JAVELIN case, the maximum thrust is provided in tabular values as a function of TAS and of the shaft rotation speed ω, moderated by the local ρ.

As the Javelin UAS is piston-powered, the fuel flow FF is computed using the following empirical model that interpolates the experimental data for the Javelin UAS consistently with [25]:

$$FF(\tau) = -1.563\tau^2 FF_{Max} + 2.5\tau FF_{Max} \tag{14}$$

Table 3 summarizes the fundamental design characteristics of RMIT's JAVELIN UAS.

3.2 Direct Transcription and Numerical Solution Algorithms

The OCP formulation offers a variety of advantages in realistic 4D guidance scenarios such as the ones investigated here. For instance, optimal control-based techniques allow accurate continuous curved descent profiles for short final GNSS approaches to be natively generated as well as optimized path stretching to be determined as necessary to achieve the set constraints for Terminal Sequencing and Spacing (TSS). Direct transcription methods are preferred as they are more capable of handling complex trajectory optimization problems. In these methods, the continuous system dynamics are transcribed into a number of discretized state and command parameters, so that a

Table 3 Assumed JAVELIN technical specifications [6]

Parameter	Value
Maximum take-off mass (m_{Max})	15 kg
Dry mass (m_{Min})	8.7 kg
Wingspan (λ)	1.8 m
Aspect ratio (AR)	11
Lift coefficient at minimum drag (c_{LminD})	0.33
Minimum drag coefficient (c_{Dmin})	0.03
Lift coefficient derivative ($c_{L,\alpha}$)	4.97 /rad
Propeller radius (r_{Prop})	0.254 m
Oswald coefficient (e)	0.75
Maximum airspeed (v_{Max})	37 m/s
Engine displacement (V)	20 cm^3
Maximum power (P_{Max})	1.28 kW
Fuel capacity (m_{Fuel})	2 kg
Endurance (t_{Max})	2 hours

system of nonlinear equations can be obtained by implicit integration along a set of time intervals. The original OCP is therefore transformed into a finite-dimensional nonlinear optimization problem. Direct collocation methods adopt piecewise polynomial functions to parameterize both states and control. The most computationally efficient class of collocation methods adopts linearly independent N-th order polynomial functions and for this reason are called Pseudo-Spectral Methods (PSM) [3, 4, 19]. These interpolation polynomials must be an orthogonal basis in the discretised space, i.e., they satisfy the null scalar product property:

$$P_i\left(x_j\right) * P_k\left(x_l\right) = 0 \,\forall\, i \neq j, \forall\, k, l \in \{1, \ldots N+1\} \tag{15}$$

The best implementations in terms of computational efficiency adopt simple interpolation polynomials in conjunction with a careful selection of the distribution of the $N+1$ collocation nodes [19]. For such reasons, Lagrange polynomials are frequently adopted for the interpolation of states and controls and a Gaussian quadrature rule is adopted for exact implicit integration. Assuming τ to be the scaled non-dimensional time and adopting the interpolation polynomials $P_k(\tau)$ on the time intervals τ_k, the states are approximated as:

$$\tilde{x}_i(\tau) = \sum\nolimits_{k=1}^{N} \tilde{x}_i(\tau_k) \cdot P_{i,k}(\tau) \tag{16}$$

and the controls are approximated as:

$$\tilde{u}_j(\tau) = \sum\nolimits_{k=1}^{N} \tilde{u}_j(\tau_k) \cdot P_{j,k}(\tau) \tag{17}$$

Lagrange polynomials of order N are expressed as:

$$P_k(\tau) = \prod\nolimits_{j \neq k} \frac{\tau - \tau_j}{\tau_k - \tau_j}, \forall\, j \in [0, N] \tag{18}$$

Chebychev PSM involve the evaluation of the N-th order Chebyshev trigonometric polynomials:

$$P_N(\tau) = \cos\left(N \cos^{-1} \tau\right) \tag{19}$$

in the $N+1$ nodes:

$$\tau_k = \cos\frac{k\pi}{N}, k \in [0, N]. \tag{20}$$

Two recently adopted PSM variants are the Gauss PSM and the Legendre-Gauss-Lobatto (LGL) PSM [1]. Gauss PSM are based on the Gauss-Legendre quadrature, whereas the LGL PSM are based on the LGL quadrature, also simply known as Lobatto quadrature. Gauss PSM are conceived to ensure that the Karush-Kuhn-Tucker (KKT) conditions are identical to the discretised first-order optimality conditions. Legendre polynomials may be calculated by using the Rodrigues formula:

$$P_N(\tau) = \frac{1}{2^N k!} \frac{d^{(N)}}{d\tau^{(N)}}\left[\left(\tau^2 - 1\right)^N\right] \tag{21}$$

The Legendre-Gauss-Lobatto (LGL) nodes are the $N+1$ zeros of the polynomial:

$$L_N(\tau) = (1 - \tau^2)\dot{P}_N(\tau) \tag{22}$$

where $\dot{P}_N(\tau)$ is the first derivative of the Legendre polynomial of degree N [5]. In Gauss PSM the dynamic constraints are not collocated at the boundary nodes, whereas in the LGL PSM the evaluation of states and controls is performed also at the boundary nodes, thereby the dimension of the NLP problem is increased by 2 additional nodes.

Based on the literature [19], the Radau PSM was selected for the GNSS loss less trajectory planning. This widely used method employs orthogonal collocation and Gaussian quadrature implicit integration, where collocation is performed at the Legendre-Gauss-Radau points. Publicly available pseudospectral optimal control solvers were chosen due to their suitability for aerospace applications. The user can also define a number of parameters used in the optimization process, including the quadrature mesh characteristics, the maximum number of iterations and the numerical differentiation method. The suitability of these techniques for ATM and Air Traffic Flow Management (ATFM) online strategic and tactical operations [14] has been demonstrated in recent research [12]. The pseudospectral transcription process of the general OCP formulated in the previous sections commences with the introduction of the following transformation:

$$\tau = \frac{2}{t_f - t_0} t - \frac{t_f + t_0}{t_f - t_0}, t \in [t_0, t_f] \tag{23}$$

The solution process is now to find the state and control trajectories $x(\tau)$ and $u(\tau)$ respectively, in the

interval $\tau \in [-1, 1]$, and times t_0 and t_f, minimizing the performance index

$$J = \phi[x(1), t_f] + \frac{t_f - t_0}{2} \int_{-1}^{1} L[x(\tau), u(\tau), \tau] d\tau \quad (24)$$

subject to the following constraints and bounds:

$$\dot{x}(\tau) = \frac{t_f - t_0}{2} f[x(\tau), u(\tau), \tau], \tau \in [-1, 1] \quad (25)$$

$$h_l \leq h[x(\tau), u(\tau), \tau] \leq h_u, \tau \in [-1, 1] \quad (26)$$

$$e_l \leq e[x(-1), x(1), u(-1), u(1), t_0, t_f] \leq e_u \quad (27)$$

$$u_l \leq u(\tau) \leq u_u, \tau \in [-1, 1] \quad (28)$$

$$x_l \leq x(\tau) \leq x_u, \tau \in [-1, 1] \quad (29)$$

$$t_{0l} \leq t_0 \leq t_{0u} \quad (30)$$

$$t_{fl} \leq t_f \leq t_{fu} \quad (31)$$

$$t_f - t_0 \geq 0. \quad (32)$$

Subdividing the continuous time domain in $N + 1$ intervals τ_k, the original continuous functions $f(t)$ can be approximated by a unique polynomial $p(\tau_k)$ of degree N whose evaluations at the intervals correspond to the values of the original function, as in [9]:

$$f(\tau_k) = p(\tau_k) \text{ for } k = 0, 1, \ldots, N \quad (33)$$

A system of Lagrange polynomials $\{p_k\}_{k=0,1,\ldots}$ (with degree k) are adopted in Eq. 33, given by:

$$P(\tau) = \sum_{k=0}^{N} f(\tau_k) L_k(\tau) \quad (34)$$

where

$$L_k(\tau) = \prod_{\substack{k \neq l \\ 0 \leq k, l \leq N}} \frac{(\tau - \tau_k)}{(\tau_l - \tau_k)} \quad (35)$$

These are mutually orthogonal over the interval $(-1, 1)$ with respect to a weight function $w \neq 0$ [7]:

$$\int_{-1}^{1} p_k(\tau) p_m(\tau) w \, \mathrm{d}\tau = 0 \text{ when } m \neq k \quad (36)$$

The use of polynomial interpolation to approximate a function using the LGL points is known in the literature as the Legendre pseudospectral approximation method. In the Legendre pseudospectral approximation, the state and control trajectories $x(\tau)$ and $u(\tau)$ respectively, in the interval $\tau \in [-1, 1]$, are approximated by N^{th} order Lagrange polynomials $x^N(\tau)$ and $u^N(\tau)$ based on interpolation at the Legendre-Gauss-Lobatto nodes [9]:

$$x(\tau) \approx x^N(\tau) = \sum_{k=0}^{N} x(\tau_k) \varphi_k(\tau) \quad (37)$$

$$u(\tau) \approx u^N(\tau) = \sum_{k=0}^{N} x(\tau_k) \varphi_k(\tau) \quad (38)$$

where $x^N(\tau)$ and $u^N(\tau)$ are the Lagrange interpolating polynomials, and $\varphi_k(\tau)$ are known as Lagrange basis polynomials. It should be noted that $\varphi_k(\tau_j) = 1$ if $k = j$ and $\varphi_k(\tau_j) = 0$ if $k \neq j$ such that:

$$x^N(\tau_k) = x(\tau_k) \text{ and } u^N(\tau_k) = u(\tau_k). \quad (39)$$

The derivative of the state vector is approximated as follows:

$$\dot{x}(\tau_k) \approx \dot{x}^N(\tau_k) = \sum_{i=0}^{N} D_{ki} x(\tau_i), i = 0, 1, \ldots, N \quad (40)$$

where D is $(N + 1) \times (N + 1)$ differentiation matrix corresponding to the LGL nodes.

The objective function of the OCP is therefore approximated as follows:

$$J \approx \phi[x^N(1), t_f] + \frac{t_f - t_0}{2} \sum_{k=0}^{N} L[x^N(\tau_k), u^N(\tau_k), \tau_k] \omega_k \quad (41)$$

where the weights ω_k are defined at the LGL nodes.

For a practical implementation, some additional considerations have to be followed. The new trajectory determined by the UAS guidance module shall be completely flyable by the aircraft systems/pilots and the mission defined in the FMS flight plan shall not be compromised by the new trajectory. Additionally, the new trajectory shall not lead to other hazards like terrain, traffic or weather. These requirements are implemented in the 4DT optimization algorithm by suitable models and a solution is pursued through the Pseudo-Spectral Optimization (PSO) method, which shows very impressive computational performances. The 4DT optimization algorithm considers the controlled time of arrival target defined by ATM, FMS or ABAS. This is used as the final time constraint by the 4DT optimization algorithm. An Estimated Time of Arrival (ETA), on the other hand, may be computed for each intermediate fix along the flight path. To further enhance the algorithm stability and convergence performances, path constraints and boundary conditions are automatically strengthened on all state and control variables to restrict the search domain as much as feasible.

3.3 Multi-objective Optimality

Conflicting objectives arising when introducing multiple operational criteria, which require multi-objective articulation of preference schemes, also known as multi-criteria decision methods. An a priori articulation of preference scheme (also known as *scalarization* technique) was selected to combine multiple objectives into an individual one that the trajectory optimization algorithm will pursue, as this choice supports efficient implementations of non-population-based optimization algorithms. Among the various possible a priori schemes, the weighted product was

Fig. 3 JAVELIN UAS 3D model

selected [17]. An advantage of this formulation compared to the more popular weighted sum is the diminished sensitivity on the absolute values of the cost terms, which proves useful when the range of the objective function is unknown or unbounded [12]. Known limitation, on the other hand, include a high probability of incurring in numerical saturation and a higher complexity of the cost function seen by the solution algorithm. Adopting the weighted product, the combined performance index is expressed as a product of all the cost terms, to the power of the assigned weight w_i, as in:

$$\tilde{J} = \prod_{i=1}^{n_J} [Q_i(\boldsymbol{p})]^{w_i} \tag{42}$$

To avoid mathematical singularities the following condition on non-null cost terms shall be enforced:

$$Q_i(\boldsymbol{p}) > 0, \forall i \tag{43}$$

In general, a specific performance objective can be defined for each route segment. This performance objective is a multi-objective generalization of the Cost Index (CI) implemented in current generation FMS. Also, in general, the weightings can be varied dynamically among the different phases of the flight. Since computational times are a crucial aspect in online 4DT planning applications, an a priori articulation of preference involving the weighted product of the various performance indexes J_i is employed to combine the multiple conflicting operational, economic and environmental objectives. For a more detailed discussion, the reader is referred to Gardi et al. [12].

The conventional fuel and time objectives are adopted here to show-case the capabilities of the implemented UAS guidance algorithm, whereas the GNSS signal loss mitigation criteria are formulated as path constrains based on CF/WF criteria (Tables 1 and 2) presented in Section 2, and in particular:

- With 5 satellites in view, the elevation angle for each satellite tracked shall be 5 degrees greater than the threshold value causing the activation of any CF;
- With 4 satellites in view, the elevation angle for each satellite tracked shall be 10 degrees greater than the threshold value causing the activation of any CF;
- The minimum elevation of any GNSS satellite is set to 5 degrees.

4 Simulation Case Studies

Some detailed simulation case studies were performed adopting the JAVELIN UAS as reference platform and evaluating the performance of the GNSS-lossless guidance algorithm described in the previous sections. The investigation focused on curved and segmented GNSS approaches. The relevant geometric, aerodynamic and inertial characteristics were retrieved to implement detailed 3D shape model and 3-DoF/6-DoF flight dynamics models of this UAS [6]. The geometric characteristics were summarized in Table 3 and the 3D CATIA model is shown in Fig. 3. For the avionics GPS receiver characteristics, we used a C/A code receiver with a flat random vibration power curve from 20 to 2000

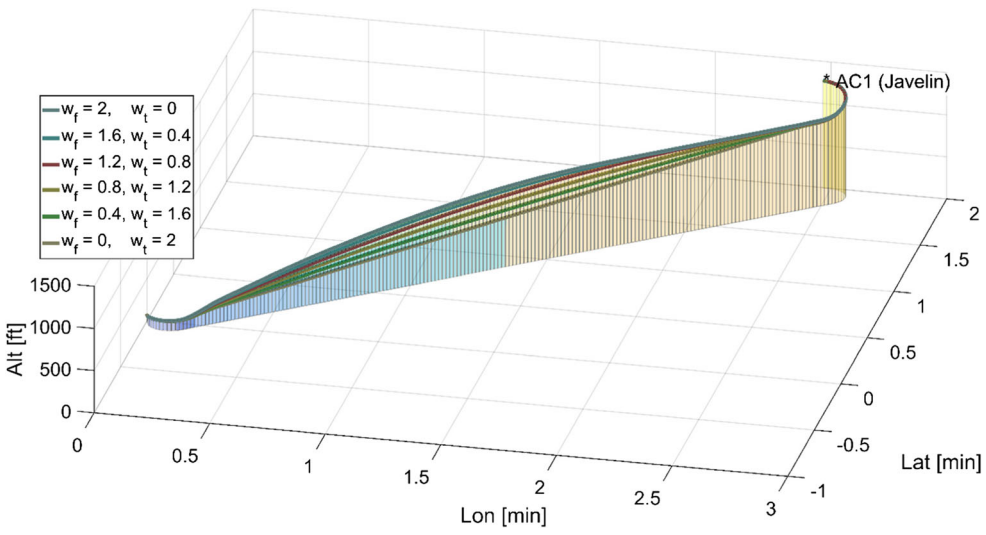

Fig. 4 Original arrival trajectories without GNSS optimization criteria

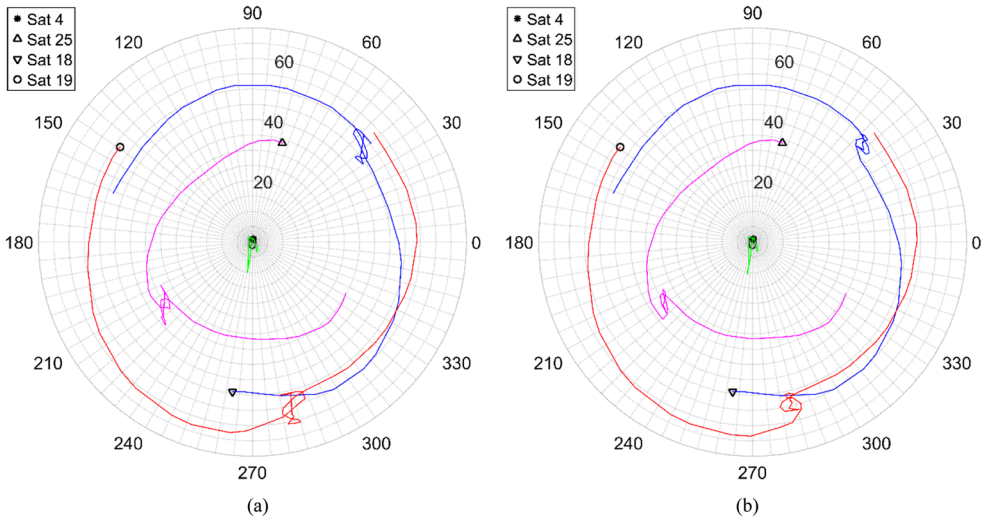

Fig. 5 Sky plots for the original minimum fuel (**a**) and minimum time (**b**) intents

Hz with amplitude of 0.005 g^2Hz^{-1} and the oscillator vibration sensitivity $S_\upsilon(f_m)= 1\times10^{-9}$ parts/g. Additionally, a third-order loop noise bandwidth of 18 Hz was considered and a maximum LOS jerk dynamic stress of 10 gs^{-1} = 98 ms^{-3} was assumed. Finally, the following simplified antenna gain pattern was adopted:

$$G_R(dB) = 7.8659 * \sin E - 4.3659 \tag{44}$$

The initial point of the arrival trajectory is set in proximity of the Waranga Basin UAS flight test range, defined as the Melbourne Flight Information Region (FIR) Danger Area YMMM D-333 - WGS84 coordinates 36.5° S 145.1° E. The initial altitude is set at 1277 ft Above Ground Level (AGL), while the final approach fix is set approximately 3 nautical miles (nmi) to the southwest at an altitude of 76.7 ft AGL. The initial conditions of the aircraft are set to a trimmed descent flight. The GPS constellation available is simulated using the YUMA almanac data. As discussed previously, the availability of GBAS at the considered location is assumed, though the MOTO-based guidance techniques presented in this paper can be equally applied to LPV and APV approaches. In this case, the final approach will have to rely on Vision-Based Navigation (VBN) or line-of-sight remote control by the ground pilot as the performance of GNSS navigation alone will not ensure a safe alignment with the runway [22]. The original 4DT intents were calculated using the pseudospectral MOTO algorithm described in the previous section in a MATLAB prototyping environment running on a consumer-grade PC equipped with an Intel i7 quad-core processor and 8 GB RAM. Figure 4 depicts the descent 4D trajectories calculated without considering the GNSS lossless constraints and Fig. 5 shows the corresponding sky plots in the antenna relative reference frame of the four satellites characterized by the maximum elevation for the minimum fuel (5a) and minimum time (5b) intents. w_f and w_t represent the fuel and time weightings used in Eq. 42 and 43 respectively. These sky plots highlight the substantial variations in elevation angles affecting all four satellites, exceeding 20 degrees relative to the initial elevation,

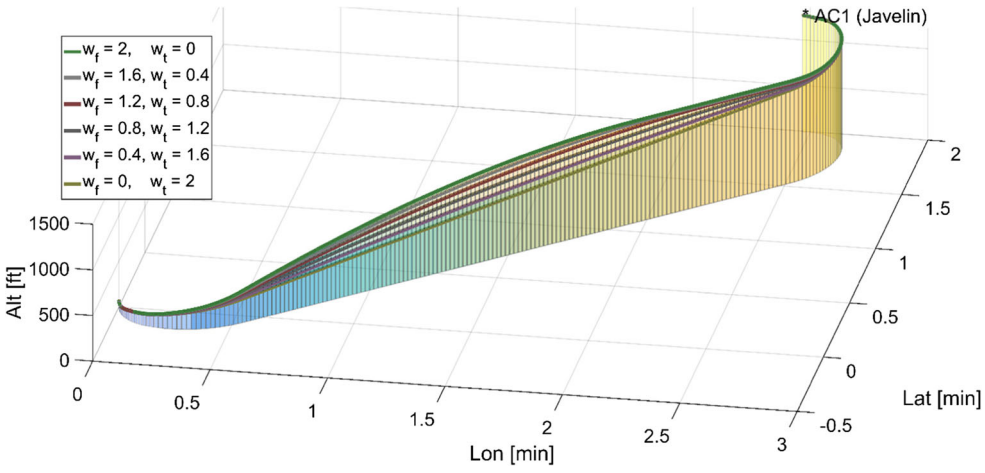

Fig. 6 Optimal arrival trajectories fulfilling GNSS optimization criteria

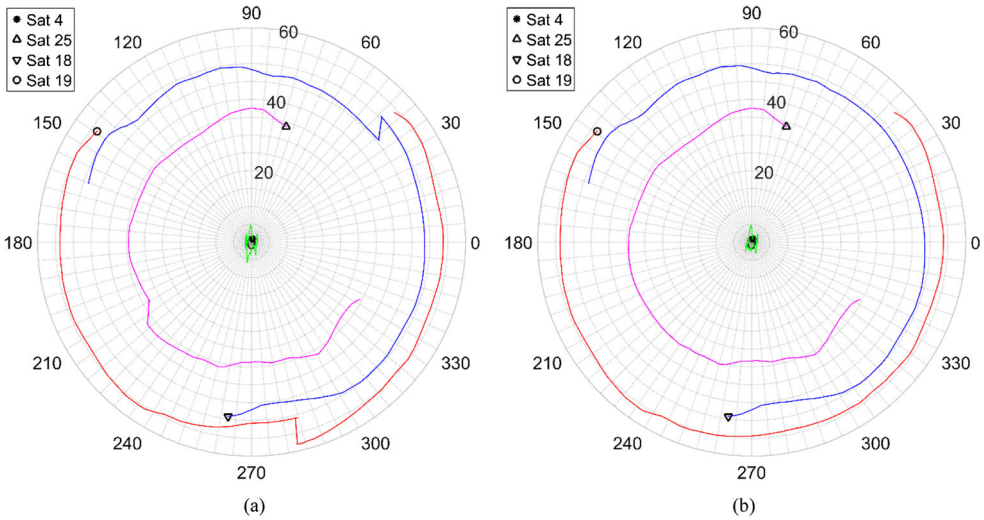

Fig. 7 Sky plots for the optimal GNSS lossless minimum fuel (**a**) and minimum time (**b**) intents

potentially affecting the PDOP and compromising the successful completion of a curved GNSS approach.

Figure 6 shows the trajectories resulting from the optimization process considering the elevation angle constraints specified in Section 2, and namely that deviations from the initial value shall not exceed the interval $[-5°; +10°]$ throughout the entire trajectory. In particular, as in the case of the original intents, six trajectories were generated as a

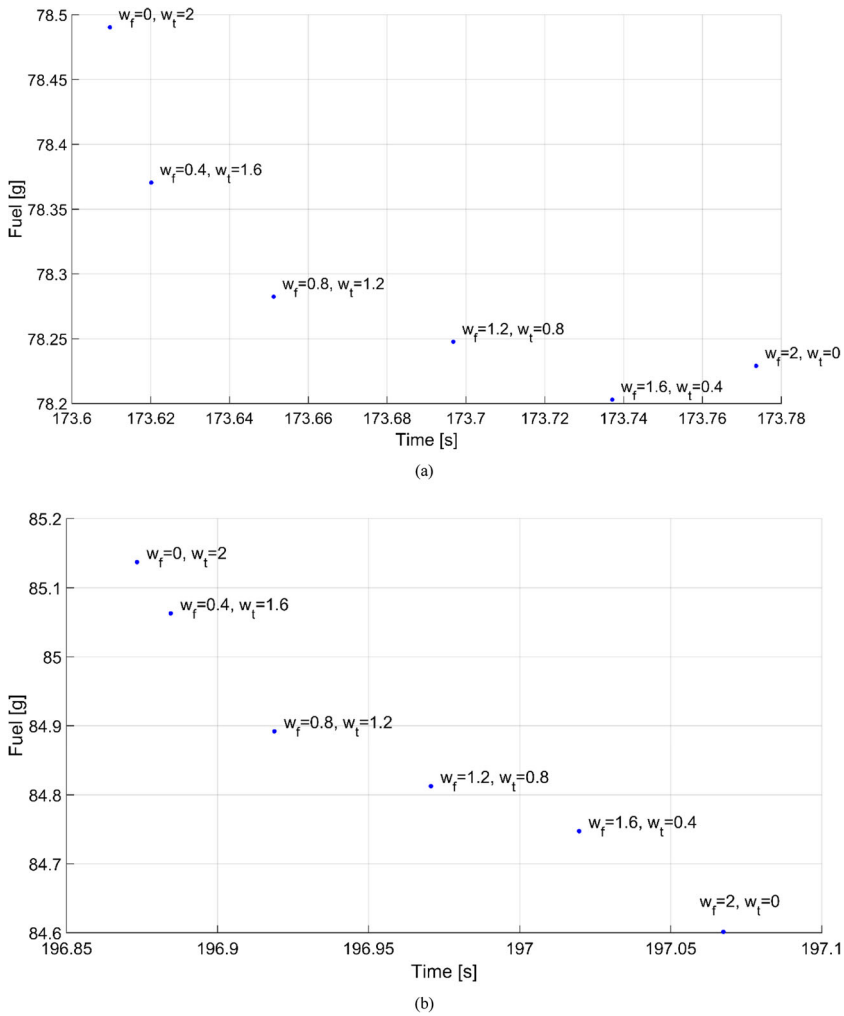

Fig. 8 Fuel and time performance respectively associated to the original intents (**a**) and to the GNSS lossless intents (**b**)

function of the relative weightings given to the fuel and time costs, w_f and w_t respectively, as specified in the legend. In this case, the number of intervals was set to 155 and the optimization processes took 49 s on average to complete. By halving the number of intervals to 79, hence relinquishing some of the accuracy in the solution, the calculation time decreases to below 16 s. Since this number of intervals still provides a very good resolution, it was used in all subsequent calculations. Figure 7 depicts the sky plots of the same four satellites in the antenna reference frame associated with the minimum fuel (7a) and minimum time (7b) intents. It is evident that the variations in satellite elevation are now significantly mitigated, remaining in a 10-degree band around the initial elevations.

Finally, Fig. 8 represents a comparison of the original Pareto front (8a) against the one associated with GNSS lossless trajectories (8b). With respect to equations (42) and (43), the figure details the weightings associated with time and fuel performances, respectively w_f and w_t, which were used for the calculation, ranging from 0 to 2 in steps of 0.4. While both fuel and time performance are by approximately 10% worse as a result of the longer and shallower flight profiles, these performance degradations are unavoidable from the safety perspective. Further simulations showed that by reducing the length of the arrival segment from 3 to 2 nmi and enforcing tighter path constraints on the control variables, the average time required for the pseudospectral MOTO process was decreased below 4 s. It is therefore concluded that an efficient exploitation of the ABAS model-predictive features and the adoption of pseudospectral algorithms in the UAS guidance module allows fulfilling the requirements for UAS guidance in terminal flight phases, potentially meeting GNSS performance requirements for curved GNSS approaches.

5 Conclusions and Future Work

This paper addressed in detail the Multi-Objective Trajectory Optimization (MOTO) algorithm developed to prevent a number of Global Navigation Satellite Systems (GNSS) signal degradation and losses in Unmanned Aircraft Systems (UAS) guidance applications. The algorithm exploits the predictive features implemented in Aircraft Based Augmentation Systems (ABAS) to avoid the occurrence of GNSS signal degradations, thereby supporting high integrity applications including precision approach and landing. After summarizing the various causes of GNSS signal degradations or losses, geometric trajectory constraints were defined in terms of satellite elevation angles in the antenna frame, as these constraints allow to address some of the most significant signal degradation and loss effects at once. Adopting these criteria and adequate forms of the aircraft dynamics models, an approach based on a multi-objective and multi-constrained optimal control problem formulation and on a pseudospectral MOTO solution algorithm was selected. Simulation case studies were accomplished on the JAVELIN UAS to verify the suitability of the proposed techniques in realistic operational scenarios, particularly focusing on terminal flight guidance for curved precision GNSS approaches. The implemented pseudospectral MOTO technique converged to a mathematical optimum within 7 to 16 s on average depending on the length and complexity of the flight path to be optimized. Further research is focussing on the following areas:

- Assess the potential synergies between ABAS and RAIM technologies, particularly looking at enhanced RAIM (eRAIM) and predictive RAIM (pRAIM) in a multi-constellation GNSS environment.
- Extend the ABAS concept to other Communication Navigation and Surveillance (CNS) applications in the CNS/Air Traffic Management (ATM) and Avionics (CNS+A) context.
- Evaluate the potential of ABAS to enhance the performance of next generation CNS+A decision support tools for Performance/Intent Based Operations (PBO/IBO) and 4DT management.
- Further investigate the potential of ABAS to support UAS SAA applications in the UAS Traffic Management (UTM) context.

References

1. Basset, G., Xu, Y., Yakimenko, O.A.: Computing short-time aircraft maneuvers using direct methods. J. Comput. Syst. Sci. Int. **49**(3), 481–513 (2010)
2. Bearman, P., Gardner, R., Green, J., Maynard, G., et al.: Air Travel - Greener By Design - Annual Report 2014–2015. RAeS, London (2015)
3. Ben-Asher, J.Z.: Optimal control theory with aerospace applications. In: American Institute of Aeronautics and Astronautics (AIAA). Reston (2010)
4. Betts, J.T.: Practical Methods for Optimal Control and Estimation Using Nonlinear Programming. SIAM, Philadelphia (2010)
5. Brix, K., Canuto, C., Dahmen, W.: Legendre-Gauss-Lobatto grids and associated nested dyadic grids. In: Aachen Institute for Advanced Study in Computational Engineering Science (2013)
6. Burston, M., Sabatini, R., Gardi, A., Clothier, R.: Reverse engineering of a fixed wing unmanned aircraft 6-DoF model based on laser scanner measurements. In: 2014 IEEE International Workshop on Metrology for Aerospace, MetroAeroSpace 2014 Proceedings, Benevento (2014)
7. Canuto, C., Hussaini, M.Y., Quarteroni, A., Zang, T.A.: Spectral Methods—Fundamentals in Single Domains. Springer, Berlin (2007)
8. CASA: Navigation authorisations: APV Baro-VNAV. In: Civil Aviation Safety Authority (CASA) of Australia Advisory Circular AC 91U-II. Canberra (2012)

9. Chircop, K., Gardi, A., Zammit Mangion, D., Sabatini, R.: A new computational technique for the generation of optimised aircraft trajectories. Nonlinear Eng. **6**(4), 249–262 (2017)
10. den Boer, R., Beers, C., Sanchez Escalonilla, P., Gomez de Segura, A., et al.: SOURDINE II Final Report (2006)
11. Gardi, A., Sabatini, R.: Descent 4D trajectory optimisation for curved GNSS approaches. In: 2017 International Conference on Unmanned Aircraft Systems. ICUAS, Miami (2017)
12. Gardi, A., Sabatini, R., Ramasamy, S.: Multi-objective optimisation of aircraft flight trajectories in the ATM and avionics context. Prog. Aerosp. Sci. **83**, 1–36 (2016)
13. Khardi, S., Abdallah, L.: Optimization approaches of aircraft flight path reducing noise: comparison of modeling methods. Appl. Acoust. **73**(4), 291–301 (2012)
14. Kistan, T., Gardi, A., Sabatini, R., Ramasamy, S., et al.: An evolutionary outlook of air traffic flow management techniques. Prog. Aerosp. Sci. **88**, 15–42 (2017)
15. Kuenz, A., Mollwitz, V., Korn, B.: Green trajectories in high traffic TMAS. In: 26th DASC Digital Avionics Systems Conference—4-Dimensional Trajectory-Based Operaions: Impact on Future Avionics and Systems, pp. 1B21–1B211. Dallas (2007)
16. Margaria, D., Falletti, E., Acarman, T.: The need for GNSS position integrity and authentication in ITS: conceptual and practical limitations in urban contexts. In: 2014 IEEE Intelligent Vehicles Symposium, IV 2014, Proceedings, pp. 1384–1389. Dearborn (2014)
17. Marler, R.T., Arora, J.S.: Survey of multi-objective optimization methods for engineering. Struct. Multidiscip. Optim. **26**(6), 369–395 (2004)
18. Mujumdar, A., Padhi, R.: Evolving philosophies on autonomous obstacle/collision avoidance of unmanned aerial vehicles. J. Aerosp. Comput. Inf. Commun. **8**(2), 17–41 (2011)
19. Rao, A.V.: Survey of numerical methods for optimal control. Adv. Astronaut. Sci. **135**, 497–528 (2010)
20. Rotondo, G.: Processing and Integrity of DC/DF GBAS for CAT II/III Operations. Institut Nationale Polytechnique de Toulouse (INP Toulouse), Toulouse (2016)
21. Sabatini, R., Moore, T., Hill, C.: Avionics-based GNSS integrity augmentation synergies with SBAS and GBAS for safety-critical aviation applications. In: 35th DASC Digital Avionics Systems Conference, DASC 2016. Sacramento (2016)
22. Sabatini, R., Moore, T., Ramasamy, S.: Global navigation satellite systems performance analysis and augmentation strategies in aviation. Prog. Aerosp. Sci. **95**, 45–98 (2017)
23. Toebben, H.H., Mollwitz, V., Bertsch, L., Geister, R.M., et al.: Flight testing of noise abating required navigation performance procedures and steep approaches. Proc. Inst. Mech. Eng. Part H: J. Aerosp. Eng. **228**(9), 1586–1597 (2014)
24. Tsourdos, A., White, B., Shanmugavel, M. (eds.): Cooperative Path Planning of Unmanned Aerial Vehicles. Wiley, Chicester (2011)
25. Yu, B., Shu, W., Bian, W.: Research on modelling of aviation piston engine for the hardware-in-the-loop simulation. Mater. Sci. Eng. **157**, 012004 (2016)

Alessandro Gardi received his BSc and MSc degrees in Aerospace Engineering from the Polytechnic University of Milan (Italy) and a PhD in the same discipline from RMIT University (Melbourne, Australia). Dr Gardi is currently the THALES Research Fellow in the School of Engineering of RMIT University, working on Air Traffic Management (ATM) system evolutions. Before joining RMIT, he was a doctoral researcher in Avionics and CNS/ATM systems at Cranfield University (United Kingdom) and a member of the Systems for Green Operations - Integrated Technology Demonstrator (SGO-ITD) research group of the Clean Sky Joint Technology Initiative for Aeronautics and Air Transport, an initiative funded under the European Union Seventh Framework Programme (EU FP7). Dr Gardi is a member of the Intelligent Transport and Mission Systems research group of RMIT University and has over 6 years of R&D experience in aerospace engineering.

Roberto Sabatini is a Professor of Aerospace Engineering and Aviation at RMIT University (Australia) with more than 25 years of experience in the aerospace/defence industry and in academia. He is an expert in avionics, Air Traffic Management (ATM) and Unmanned Aircraft Systems (UAS), with specific hands-on competence in flight Guidance, Control and Dynamics (GCD), aeronautical Communication, Navigation and Surveillance (CNS), aviation human factors engineering, and multi-sensor data fusion for civil and military applications. Currently, Prof. Sabatini is Head of the Intelligent Transport and Mission Systems Group and Research Program Leader for Aviation/Aerospace Systems at RMIT University. Prof. Sabatini is a Fellow of the Royal Aeronautical Society and of the Royal Institute of Navigation, a Senior Member of IEEE and AIAA, and a Life Member of AFCEA.

Dr. Subramanian Ramasamy obtained his postgraduate degree in Aerospace Engineering (specialisation in Avionics) from Madras Institute of Technology (India). Prior to pursuing his PhD, he was working at THALES, gaining hands-on experience in Flight Management Systems and Human Machine Interfaces. At Cranfield University (UK), he was part of the Systems for Green Operations Integrated Technology Demonstrator (SGO-ITD) of the Clean Sky Joint Technology Initiative (JTI) for Aeronautics and Air Transport research group. After obtaining his doctorate at RMIT University (Australia), he is currently continuing his research at his alma mater. His areas of interest are aeronautical Communication, Navigation and Surveillance (CNS) systems, Unmanned Aircraft Systems (UAS), Traffic Management for UAS and Cognitive Ergonomics for aerospace applications.

Mr. Trevor Kistan is the Research & Technology Manager at THALES Australia Air Traffic Management division where he oversees research initiatives in Air Traffic Management (ATM), Air Traffic Flow Management (ATFM) and Unmanned Aircraft Systems Traffic Management (UTM) systems. He has 25 years of systems and software engineering experience within the THALES group. He holds an MSc in Computer Science (specialising in Artificial Intelligence) from the University of Kwa-Zulu Natal (South Africa) and is currently pursuing a PhD in Aerospace Engineering at RMIT University (Australia) focusing on the implementation of next-generation ATFM systems. His other research interests include Communications, Navigation, Surveillance, Air Traffic Management and Avionics (CNS+A) systems, cognitive neuroscience, human factors engineering and agent-based systems.